PERGAMON

International Journal of Solids and Structures 40 (2003) 295–315

INTERNATIONAL JOURNAL OF SOLIDS and STRUCTURES

www.elsevier.com/locate/ijsolstr

On the continuous wavelet transforms applied to discrete vibrational data for detecting open cracks in damaged beams

Angelo Gentile, Arcangelo Messina *

Dipartimento di Ingegneria dell'Innovazione, Via Monteroni, Università di Lecce, Lecce 73100, Italy

Received 15 April 2002; received in revised form 10 September 2002

Abstract

This paper deals with the detection of open cracks in beam structures that undergo transverse vibrations. The investigation is aimed at detecting the location of open cracks in damaged beams by minimizing measurement data and baseline information of the structure. The study is carried out by using the continuous wavelet transform (CWT). The application of this recent, but advanced, mathematical tool is initially presented through a theoretical background, which is believed to be valuable for bridging the gap between the CWT and previous existing techniques. It is shown how the possibility to efficiently identify localized damages by CWT comes up from the intrinsic capability of the wavelets to collect several mathematical tools in only one mathematical aspect: derivatives, convolution and appropriate smoothing of data are translated into the CWT. Simulations show how the redundancy of the CWT in the functional space is able to efficiently identify locations of open cracks in the presence of noisy or clean data. Indeed, the possibility to approach the problem by using different families of wavelets, for several available scales, allows a successful application of the characteristic microscopy of the wavelets. The technique may be promisingly applied to discrete vibrational data.

Keywords: Beams; Cracks; Vibrations; Wavelet

1. Introduction

Damage detection based on using changes in modal data is becoming one of the most attractive research topics in recent years. The relevant literature is continuously increasing for the undoubted advantages offered by the modal databased techniques with respect to existing diagnostic techniques (acoustic emission, eddy current, radiographic etc.). These latter can detect a damage only in locations established a priori.

The existing modal databased techniques (e.g. Doebling et al., 1998) mainly concern natural frequencies and mode shapes. Recently, Pai and Young (2001) also took into account operative deflection shapes (ODSs) described in Døssing and Staker (1987) and McHargue and Richardson (1993). An ODS consists of a deflection shape of a structure excited through a single-frequency harmonic. The methods based on

* Corresponding author. Fax: +39-0832-320-279.
E-mail address: arcangelo.messina@unile.it (A. Messina).

0020-7683/02/$ - see front matter
PII: S0020-7683(02)00548-6

natural frequency changes have the principal attraction to make use of a reduced set of experimental data that is also easily measurable and less contaminated by experimental noise. However, mode shapes inherently possess the geometry of the system and a damage may be potentially determined by directly processing the geometric changes of the shape. The natural frequencies are also able to recover the relevant information connected with the geometry of the system; however, the recovering process is in such a case strictly related to the estimation of numerical quantities that simulate the relevant real quantities (e.g. Stubbs and Osegueda, 1990; Messina et al., 1998).

With respect to the case dealt with this paper, the first significant efforts could be historically attributed to Yuen (1985) and Pandey et al. (1991). Yuen (1985) and Pandey et al. (1991) reported that derivatives of displacements should be considered as the main tools leading diagnosing information. Indeed, the numerical simulations carried out by Yuen (1985) showed that significant changes can occur in the slopes of displacements in the proximity of the damaged locations. On the other hand, Pandey et al. (1991) discovered that a systematic detection of damaged locations in beams could be obtained by looking at certain characteristic peaks associated to the curvature mode shapes changes between intact and damaged states. Pandey et al. (1991) (similarly to Yuen, 1985) reached such conclusions by using numerical FE-models. The curvature was assessed by Pandey et al. (1991) with a classical three-point equation based on a well-known finite difference scheme. The successes obtained by the numerical simulations of Pandey et al. (1991) were not subsequently always successfully supported by the experimental tests. For example, Chance et al. (1994) reported that curvatures changes could be masked by the derivative operations in the presence of noisy data. However, other investigators (e.g. Jauregui and Farrar, 1996), in other experimental circumstances, found the mode shapes curvature changes useful damage detection indicators.

The idea of Pandey et al. (1991) was subsequently adopted by Hoerst and Ratcliffe (1997) and Ratcliffe and Bagaria (1998). These investigators aimed at detecting damaged conditions by avoiding any baseline information of the undamaged structure (a fact generally present in practice). Hoerst and Ratcliffe (1997) and Ratcliffe and Bagaria (1998) presented a method (*gapped smoothing*), which essentially aimed at extracting certain peaks, characteristic of local damages, by processing the curvature mode shape in its only damaged condition.

The method suggested by Hoerst and Ratcliffe (1997) was also applied to detect open cracks in damaged beams by Gentile and Messina (2002). In addition to the previous investigations, Gentile and Messina (2002) used the gapped smoothing method in conjunction with all the derivatives up to the third order. In particular, the numerical and experimental investigations carried out by Gentile and Messina (2002) showed how the gapped smoothing method, if applied over all the derivatives, could also be able to identify characteristic peaks of damaged conditions. The redundancy of the peaks, associated to different derivatives, could help the identification process. However, the noise still significantly affected the success of the processing techniques.

Based on all the previously mentioned investigations, the derivatives should be clearly considered useful tools for identifying cracks, with the identification which can also be obtained by processing shapes in the only damaged conditions. However, for the classical derivative operations a careful implementation has to be retained important with noisy data (Chance et al., 1994; Gentile and Messina, 2002).

In order to preserve the usefulness of the derivatives and possibly reduce the problems related with noisy data, an appropriate mathematical tool is needed. In this respect, the present investigation uses continuous wavelet transforms (CWTs) (Daubechies, 1992; Mallat and Hwang, 1992; Misiti et al., 1996; Mallat, 2001) for detecting open cracks in transversely vibrating beams. In particular, it will be illustrated from both a theoretical and numerical point of view how the CWT is able to extract the relevant information connected to the derivative of the signal (mode shapes and/or ODS) by also successfully challenging noisy data.

It is stressed that the present work does not constitute the first attempt that uses wavelets to detect cracks in beams (Surace and Ruotolo, 1994; Naldi and Venini, 1997; Wang and Deng, 1999; Lu and Hsu, 1999; Quek et al., 2001; Hong et al., 2002). Surace and Ruotolo (1994) applied the CWT only to detect the

presence of a breathing crack. To this end the complex Morlet function was used as an analyzing wavelet. The investigations carried out by Naldi and Venini (1997) and Lu and Hsu (1999) considered a discrete wavelet transform; they analyzed dynamical structural aspects on 1-D truss structures and flexible strings respectively.

As far as the interests of the present paper are concerned, the works by Wang and Deng (1999), Quek et al. (2001) and Hong et al. (2002) are mainly of interest. Wang and Deng (1999) and Quek et al. (2001) investigated the possibility of identifying the presence and the location of localized damage on transversally vibrating beams by using wavelet analysis. However, Wang and Deng (1999) used a discrete Haar wavelet transform (Haar, 1910; Daubechies, 1992) to identify the location of damage in beams and plates. Moreover, Quek et al. (2001) compared the performances of two different analyzing wavelets: Haar and the complex Gabor wavelets. The paper by Hong et al. (2002), appeared a few days before submitting the present manuscript, is further relevant. Indeed, Hong et al. (2002) used the CWT to estimate the damage location and extent by using the Lipschitz exponent (Daubechies, 1992; Holschneider, 1995; Mallat, 2001). The investigation was based on only one analyzing wavelet (i.e. the Mexican hat wavelet) by focusing the attention mainly on the fundamental mode shape.

In spite of all successes mentioned by the previous works (Surace and Ruotolo, 1994; Naldi and Venini, 1997; Wang and Deng, 1999; Lu and Hsu, 1999; Quek et al., 2001; Hong et al., 2002) the investigations were conducted without considering the possibility of correlating existing techniques with wavelets. Such a correlation should be considered of fundamental importance for supporting the reasons that should conduct the investigators to use wavelets rather than derivatives (Yuen, 1985; Pandey et al., 1991; Ratcliffe and Bagaria, 1998; Gentile and Messina, 2002). These latter are, on the other hand, more easily applicable. Moreover, whenever, the wavelets are not to be ignored in a damage detection procedure, a theoretical base assisting a possible choice among all the existing analyzing wavelets (Daubechies, 1992; Misiti et al., 1996) was not even suggested in the previous investigations. Finally, a part from the work by Hong et al. (2002) that investigated only one experimental case with a beam containing a relatively longitudinally large flaw, the investigations did not carry out numerical or experimental simulations that accounted contamination by noise.

In this work, the use of CWTs is taken into account in place of discrete ones (Naldi and Venini, 1997; Wang and Deng, 1999; Lu and Hsu, 1999; Quek et al., 2001) for detecting the location of localized defects. The paper focused on the identification of damaged locations that could be considered of primary importance in a diagnosing process. The CWTs are applied to discrete data (e.g. sampled mode shapes or ODSs) and the related results are theoretically justified. Such a theoretical justification can assist the analyst in choosing appropriate analyzing wavelets in the case of interest. It is also illustrated how an appropriate use of the wavelets translates into the advantages of the derivatives (Pandey et al., 1991; Gentile and Messina, 2002) to identify cracks. In this respect, the discrete Haar wavelet, implemented in Wang and Deng (1999) and Quek et al. (2001), cannot be considered as the best choice among the possible existing wavelets in the manner of CWT. Moreover, by combining different choices of wavelets and scales it is shown that the identification of cracks could be also obtained as a gapped smoothing method (Hoerst and Ratcliffe, 1997). Finally, an appropriate choice of scales and vanishing moments related to the wavelets seems to be able to efficiently tackle noisy data. In this latter respect, it appears that the finest scales cannot be generally considered the best choice when the presence of noise is not negligible. In passing, the present work also investigates the possibility of tackling certain problems correlated to the boundary of beams. Namely, it is shown that techniques borrowed from digital signal processing area can constitute a possible remedy to avoid singularities of CWT occurring at certain boundary conditions also for undamaged beams.

Even though all the numerical simulations are generally done on a redundant number of points, numerical examples finally show how the method is not extremely influenced by the resolution of the measurement grid. In any case, the high number of points used is chosen to be consistent with the most recent

technological systems of vibration measurement (Pai and Young, 2001), where, on the other hand, the noise can play a significant role.

2. Theory

2.1. Wavelets and mathematical microscopy: the Hölder–Lipschitz continuity

Let $y(x)$ be a signal of interest in its dimensional domain $[0, L]$. The mathematical generalization of the definition considers the function $y(x)$ defined in $]-\infty, +\infty[$. However, this does not limit our presentation due to the fact that a finite domain can be taken into consideration by assuming a windowed signal in the infinite space.

A wavelet $\psi(x)$ can be defined (Mallat, 2001) as a function having a zero average:

$$\int_{-\infty}^{+\infty} \psi(x)\,\mathrm{d}x = 0 \tag{1}$$

being $\psi(x)$ the *wavelet mother* from which the analyzing wavelets can be obtained by dilations (s: dilation parameter; real positive number) and translations ($\bar{x}$: translation parameter; real number):

$$\psi(x)_{\bar{x},s} = \frac{1}{\sqrt{s}}\psi\left(\frac{x-\bar{x}}{s}\right) \tag{2}$$

by also weighting the wavelet mother with $s^{-1/2}$. The wavelet mother can be a real or complex function. However, in this context, where the main concern is the detection of local irregularities in low wavelength signals, only real wavelets will be used. Therefore, the CWT corresponds to the following definition:

$$W(y(x);s) = Y(x;s)_W = \int_{-\infty}^{+\infty} y(x)\frac{1}{\sqrt{s}}\psi\left(\frac{x-\bar{x}}{s}\right)\mathrm{d}x \tag{3}$$

having assumed the convention to indicate any transformed quantity with a relevant capital letter (i.e. Y is the transformed quantity of y). The index of a transformed quantity (i.e. w in Y_W) will indicate the kernel of the transformation (W refers to wavelet transform, F refers to Fourier transform).

Property 1. It might be of interest to note that Eq. (3), a part from the turning over of the analyzing wavelet, corresponds (Otnes and Enochson, 1978) to a convolution of the signal $y(x)$ with the wavelet at a fixed scale s. On the other hand, the Fourier transform of the convolution of two signals corresponds to the product of both Fourier transformed signals. The following equations re-assume this property:

$$\begin{cases} Y(x;s)_W = \frac{1}{\sqrt{s}}y(x) * \psi(-x/s); \\ Y(\omega;s)_{W,F} = \sqrt{s}Y(\omega)_F \Psi(s\omega)_F \end{cases} \tag{4}$$

being "$*$" the convolution operator and ω the angular frequency [rad/dim(x)].

This property becomes useful to interpret the behavior of the wavelets in presence of Gaussian noise (Section 4). Moreover it also explains how large scales (high value of s) identify original sharp irregularities with softer peaks (Sections 3 and 4).

The vanishing moments associated with a wavelet are also of considerable concern in this work. In particular, a wavelet is said to have m vanishing moments when the following equation holds:

$$\int_{-\infty}^{+\infty} x^k \psi(x)\,\mathrm{d}x = 0, \quad k = 0, 1, 2, \ldots, m-1 \tag{5}$$

from which follows that any wavelet has at least one vanishing moment (see Eq. (1)).

Based on the definition of vanishing moments (5) the following property can be proved (Mallat, 2001).

Property 2. If a wavelet $\psi(x)$ is characterized by a fast decay and m vanishing moments it is possible to prove the existence of a function $\theta(x)$ having a fast decay whose mth derivative is related to the same $\psi(x)$ as is reported in Eq. (6).

$$\int_{-\infty}^{+\infty} x^k \psi(x)\,\mathrm{d}x = 0, \quad k = 0, \ldots, m-1 \Longleftrightarrow \text{exist } \theta(x) \text{ such that } \psi(x) = (-1)^m \frac{\mathrm{d}^m \theta(x)}{\mathrm{d}x^m} \tag{6}$$

Under condition (6), Mallat (2001) also proves that the following equation:

$$\int_{-\infty}^{+\infty} \theta(x)\,\mathrm{d}x = K \neq 0 \tag{7}$$

is a sufficient and necessary condition to state that $\psi(x)$ has no more than m vanishing moments. Finally, whenever Eqs. (6) and (7) hold, Mallat (2001) finally proves that the following equation holds:

$$\lim_{s\to 0} \frac{Y(x;s)_W}{s^{m+1/2}} = K \frac{\mathrm{d}^m y(x)}{\mathrm{d}x^m} \tag{8}$$

for an m times continuously differentiable (C^m) function $y(x)$.

Eq. (8) is of considerable importance in this work for two reasons. Firstly, once s has been fixed to a comparably small value in the domain of interest $[0, L]$, the CWT $(Y(x;s)_W)$ can be expected to be a good approximation of $Ks^{m+1/2}$ times the mth derivative of the signal $y(x)$. This statement clearly remarks the importance of choosing an appropriate wavelet mother to analyze the signal in the present context. Indeed, at the finest scales (lowest value of s) a wavelet with only one vanishing moment will derive properties from the function $y(x)$ that are related to the first derivative of the signal. This similarly happens for the higher order derivatives. Secondly, if s is considered variable, Eq. (8) stresses the importance of using an appropriate wavelet to nullify, at finest scales, the regular parts of the signal. Indeed, if a wavelet is characterized by m vanishing moments and the mth derivative of $y(x)$ is bound, Eq. (8) highlights that $Y(x;s)_W$ decays to zero with the same velocity of $s^{m+1/2}$ (say $Y(x;s)_W$ has an order of decay $\mathrm{O}(s^{m+1/2})$).

Eq. (8) together with the Hölder–Lipschitz continuity (HLc) constitutes the kernel of the microscopy characterizing the wavelets. As far as the HLc definitions are concerned, this work can only refers to Daubechies (1992), Holschneider (1995) and Mallat (2001) for brevity's sake. Here it can only be reassumed that Eqs. (6)–(8) combined with the HLc are theoretically able to relate the presence of singularities of a signal to certain local maxima that propagate at finer scales in the neighborhood of the same singularities. However, as pointed out in Mallat (2001), there is no guarantee that a rupture of the propagation of the maxima does not exist towards the finest scales. This is evidently a drawback for an analyst who should be certain that a fine scale is always, in principle, able to detect a singularity in the signal. Fortunately, Mallat (2001) also illustrates how certain wavelets (hereafter called *Gaussian wavelets*) satisfying condition (6) never cause an interruption of the maxima. For this latter reason, this work will particularly concentrate on the study of the Gaussian wavelets without neglecting to carry out relevant comparisons with other known wavelets.

2.2. Wavelets and derivatives: analytical and numerical equivalences

In Section 2.1 the CWT and related properties were introduced from an analytical point of view. In practice real functions (mode shapes) are not measured as analytical expressions. A classical measurement system as, for example, an impulse hammer (Ewins, 1992) technique is able to measure mode shapes at a few discrete points of a transversally vibrating beam. Recently Pai and Young (2001) also reported the possibility of measuring displacements on denser grids (a few hundred of points) by using a scanning laser vibrometer. In any case what we can expect from an experimental test is a list of numbers representative of discrete displacements. In such a situation a numerical algorithm can only approximately evaluate the CWT.

Due to the importance of Eq. (8) for this work, Eq. (8) is firstly analytically tested to get evidence of its accuracy when the scale is not an analytical limit for $s \to 0$. This test is carried out by using an exact Haar wavelet transform. Further simulations investigate the numerical accuracy of CWTs evaluated with respect to discrete data.

Eq. (9a) illustrates the analytical expression of a Haar wavelet (Haar, 1910). Eq. (9b) corresponds to $\theta(x)$ defined through Property 2 of the previous section. By assuming the center of the Haar wavelet as the leading point of the analyzing wavelet, the general analytical expression of Eq. (3) corresponds to Eq. (10) when the support of the signal $y(x)$ is compact in $[0, L]$ (0 outside) and the support of the Haar wavelet mother is unitary.

$$\psi(x) = \begin{cases} +1 & \text{if } 0 \leqslant x < 1/2 \\ -1 & \text{if } 1/2 \leqslant x < 1 \\ 0 & \text{otherwise} \end{cases} \tag{9a}$$

$$\theta(x) = \begin{cases} -x & \text{if } 0 \leqslant x < 1/2 \\ x-1 & \text{if } 1/2 \leqslant x < 1 \\ 0 & \text{otherwise} \end{cases} \tag{9b}$$

$$W(y(x);s) = \begin{cases} -s^{-1/2} \int_0^{x+s/2} y(z)\,\mathrm{d}z & \text{if } -s/2 \leqslant x < 0 \\ +s^{-1/2} \left[\int_0^{x} y(z)\,\mathrm{d}z - \int_x^{x+s/2} y(z)\,\mathrm{d}z \right] & \text{if } 0 \leqslant x < s/2 \\ +s^{-1/2} \left[\int_{x-s/2}^{x} y(z)\,\mathrm{d}z - \int_x^{x+s/2} y(z)\,\mathrm{d}z \right] & \text{if } s/2 \leqslant x < L - s/2 \\ +s^{-1/2} \left[\int_{x-s/2}^{x} y(z)\,\mathrm{d}z - \int_x^{L} y(z)\,\mathrm{d}z \right] & \text{if } L - s/2 \leqslant x < L \\ +s^{-1/2} \int_{x-s/2}^{L} y(z)\,\mathrm{d}z & \text{if } L \leqslant x < L + s/2 \\ 0 & \text{otherwise} \end{cases} \tag{10}$$

If the signal of interest is assumed to be $y(x) = \sin(\pi x/L)$ [1] the corresponding wavelet transform can then be analytically extracted by Eq. (10) in its closed form.

In order to illustrate the accuracy of Eq. (8) by using a finite scale s, Fig. 1 is worthy of attention. Fig. 1(a) illustrates the signal ($y(x) = \sin(\pi x/L)$) windowed in $[0, L]$ with $L = 1$ m at $x = 0.3$ m the Haar wavelet, scaled with $s = 0.2$ ($S = 0.2$ m), is also represented. Fig. 1(b) compares and shows an excellent agreement

[1] Corresponding to the first mode shape of a simply supported slender beam.

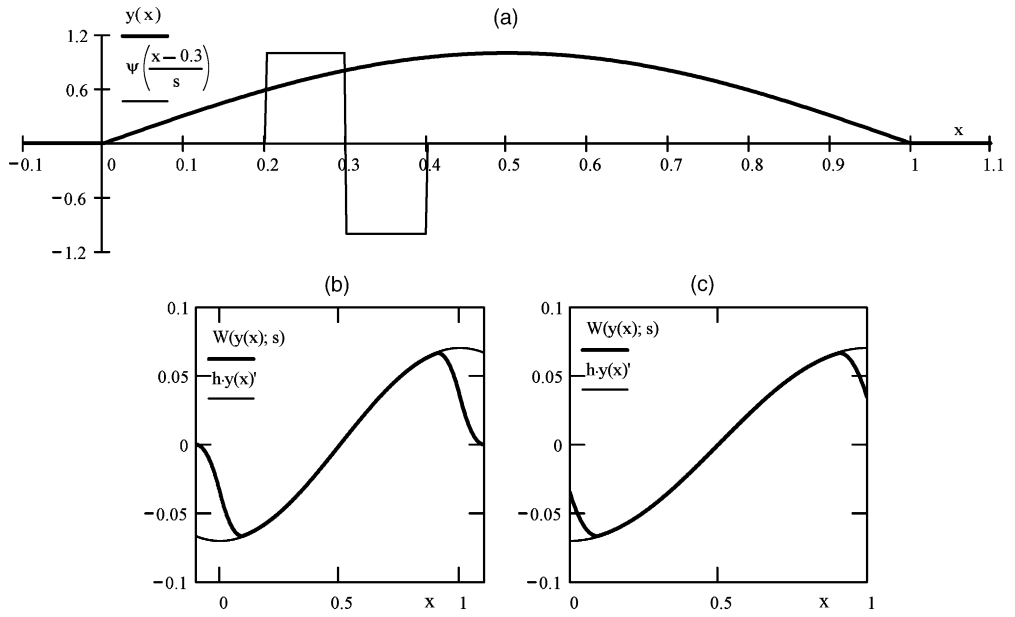

Fig. 1. Exact representations of continuous Haar wavelet transforms for the function: $y(x) = \sin(\pi x/L)$; $s = 0.2$; $L = 1$ m; $x : [0, 1]$ m.

between the analytical wavelet transform (10) and the first derivative of the function $(y(x) = \pi \cos(\pi x/L)/L)$ weighted with the factor $h = -s^{3/2}/4$ (7), (9a) and (9b). Large discrepancies at the boundaries are also evident. However, the non-agreement at boundaries cannot be considered a limitation of the wavelet transform nor can it be expected that the wavelet transform is strictly equivalent to the classical derivative; rather, the wavelet transform can include the derivatives. The large discrepancies at the boundaries depend on the fact that the analyzing wavelet convolves $y(x)$ in the infinite space, therefore the discontinuity of the CWTs at $x = 0$, L are naturally identified with a *jump* (or *peak*) due to the presence of the singularities at those points.

Finally, Fig. 1(b), as well as Eq. (10), highlights that the resulting support of the wavelet transform $Y(x)_W$ is $[-s/2, L + s/2]$. This support is larger than the support of the signal $[0, L]$. However, as the detection of singularities is the problem of main concern in this work, the partial support $[[-s/2, 0] \cup [L, L + s/2]]$ will be ignored (Fig. 1(c)) in the following investigations.

As far as the numerical estimation of the CWT is concerned, the algorithm implemented by Misiti et al. (1996) has been used in this work. In order to illustrate its numerical performance, a few tests compare the numerical estimate of CWT with the exact analytical one (10). The synthesis of this comparison is illustrated in Fig. 2 and concerns the same signal of Fig. 1. Fig. 2 illustrates that the higher the number of discrete points is, the higher is the accuracy of the estimate of the CWT. In particular, Fig. 2(b) and (d) illustrate how the overlap of both the approximate and exact evaluation of CWTs makes the relevant curves indistinguishable. However, for the cases dealt with herein, the accuracy of the numerical estimate of the CWT does not seem extremely compromised.

Finally, Fig. 3, illustrates the comparisons between five different CWT (Haar, Gaus 1–4) and the first four derivatives of the signal $y(x) = \sin(\pi x/L)$. The CWTs presented in Fig. 3 were weighted with the factor $h^{-1} = 1/K s^{m+1/2}$ which depends on the analyzing wavelet through Eq. (7). The wavelets indicated with diction Gaus 1–4 were obtained by applying Property 2 (i.e. Eq. (6, part 2) on the following modified Gaussian functions $\theta(x)_j$:

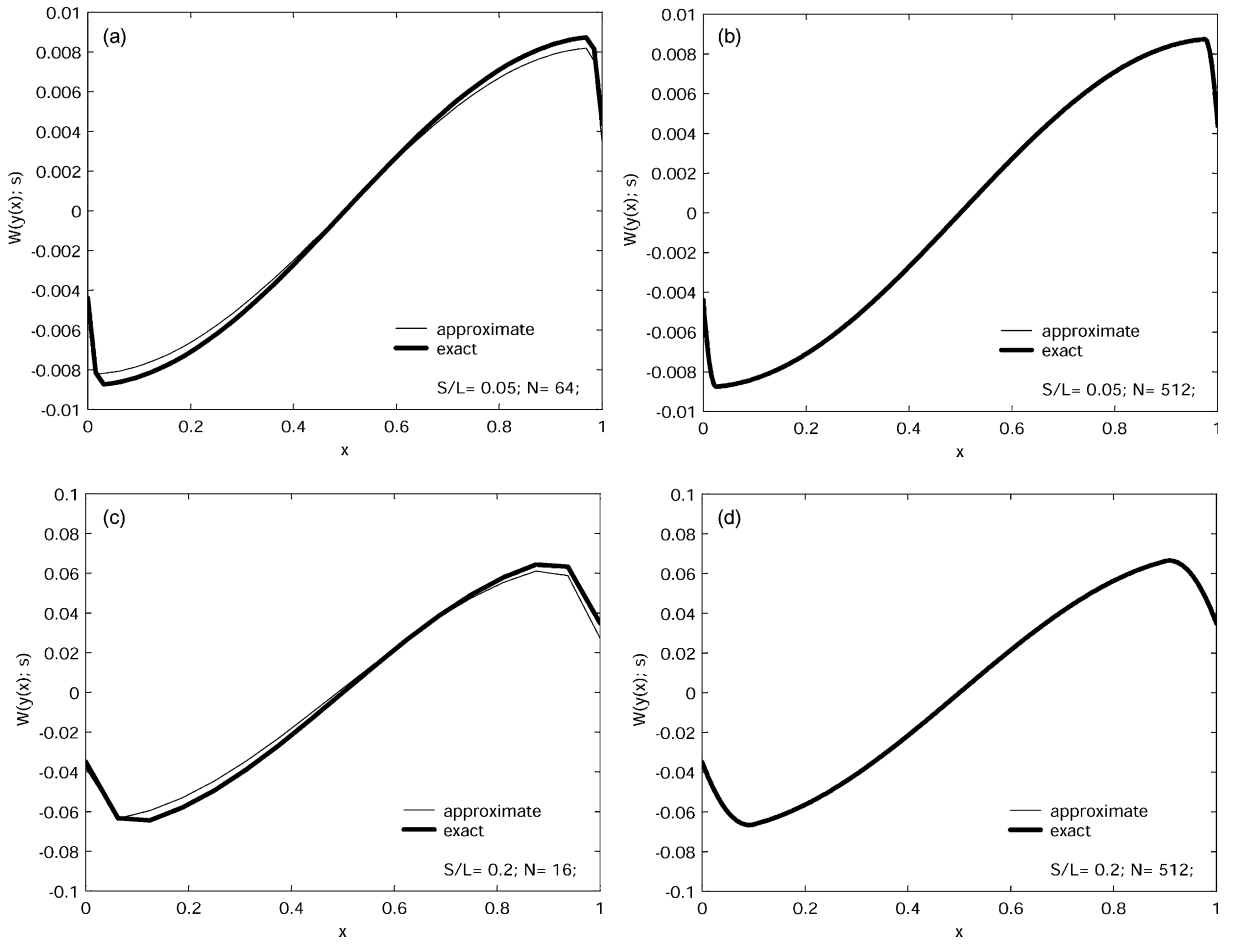

Fig. 2. Exact continuous Haar wavelet transforms versus approximate CWTs applied on discrete data: $y(x) = \sin(\pi x/L)$.

$$\begin{cases} \theta(x)_1 = -\mathrm{e}^{-x^2}\sqrt[4]{2/\pi}; & K_1 = -\sqrt[4]{2\pi} \\ \theta(x)_2 = -\mathrm{e}^{-x^2}\dfrac{\sqrt[4]{2/\pi}}{\sqrt{3}}; & K_2 = -\dfrac{\sqrt[4]{2\pi}}{\sqrt{3}} \\ \theta(x)_3 = \mathrm{e}^{-x^2}\dfrac{\sqrt[4]{2/\pi}}{\sqrt{15}}; & K_3 = \dfrac{\sqrt[4]{2\pi}}{\sqrt{15}} \\ \theta(x)_4 = \mathrm{e}^{-x^2}\dfrac{\sqrt[4]{2/\pi}}{\sqrt{105}}; & K_4 = \dfrac{\sqrt[4]{2\pi}}{\sqrt{105}} \end{cases} \tag{11}$$

whose modification of the Gaussian function was made according to the condition of having the norm of the Gaussian wavelets (12) unitary ($\int_{-\infty}^{\infty}\psi(x)_j^2\,\mathrm{d}x = 1$).

$$\begin{cases} \psi(x)_1 = (-1)^1 x\,\mathrm{e}^{-x^2} 2\sqrt[4]{2/\pi} \\ \psi(x)_2 = (-1)^2(1-2x^2)\,\mathrm{e}^{-x^2}\dfrac{2\sqrt[4]{2/\pi}}{\sqrt{3}} \\ \psi(x)_3 = (-1)^3(3x-2x^3)\,\mathrm{e}^{-x^2}\dfrac{2^2\sqrt[4]{2/\pi}}{\sqrt{15}} \\ \psi(x)_4 = (-1)^4(3-12x^2+4x^4)\,\mathrm{e}^{-x^2}\dfrac{2^2\sqrt[4]{2/\pi}}{\sqrt{105}} \end{cases} \tag{12}$$

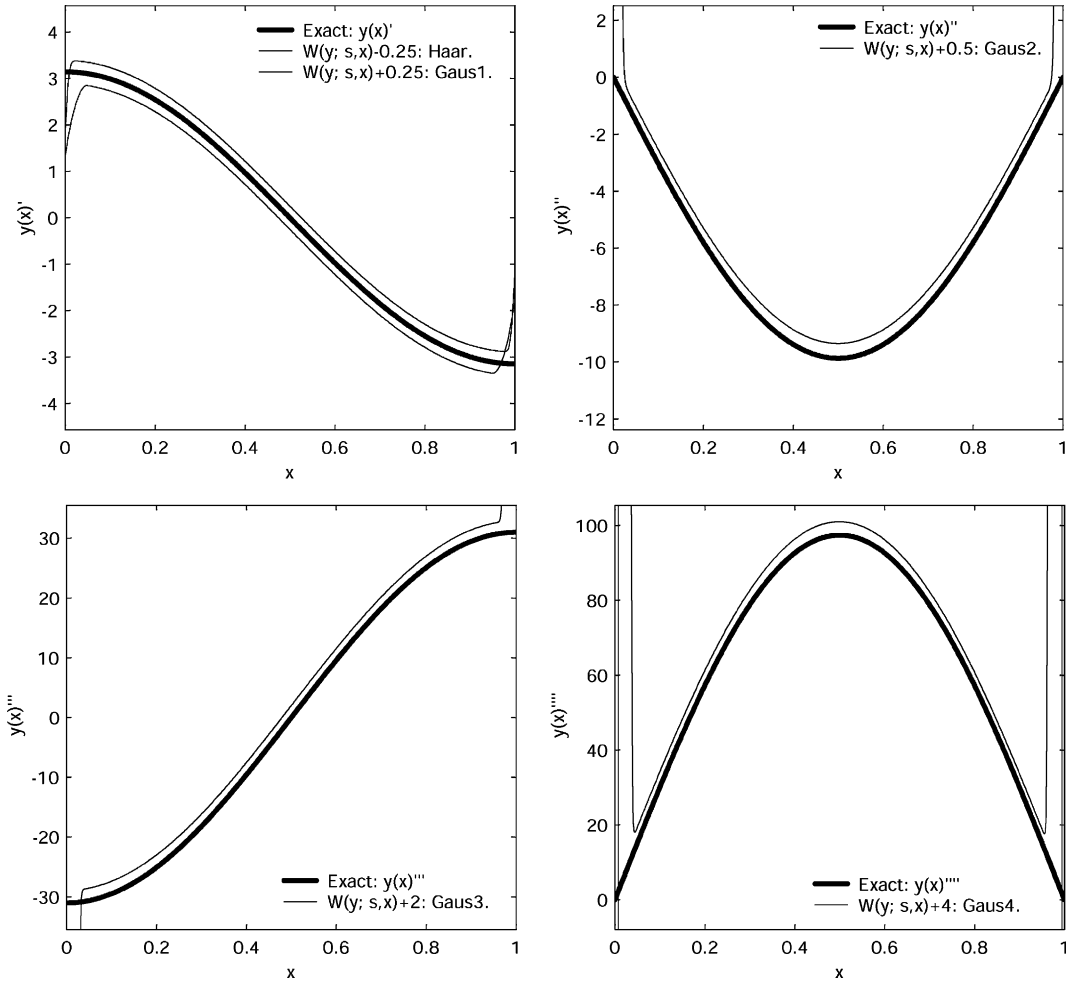

Fig. 3. Comparison between exact derivatives and CWTs based on different wavelets mother applied on discrete data: $y(x) = \sin(\pi x/L)$; $N = 512$; $S/L = 0.1$.

Each one of the wavelets represented (12) will be indicated in the following by using the diction Gaus 1–4. Due to the fact that wavelets (12) are based on Property 2 they are characterized from a number of vanishing moments that correspond to their index. Therefore, for Property 2, in particular Eq. 8, such Gaussian wavelets should be able to extract certain information from a signal that corresponds to the respective derivatives (1st, 2nd, 3rd, 4th). Such a capability is clearly shown in the above mentioned Fig. 3 that was based on wavelets assessed by using 512 discrete points. Fig. 3 finally highlights the interesting fact that the Haar wavelet is equivalent to Gaus 1 wavelet under the perspective to evaluate the first derivative of the signal. This result is consistent with the number of vanishing moments of both Haar and Gaus 1 wavelets.

Based on the good behavior of the numerical algorithm illustrated by Misiti et al. (1996), all the following estimates of the CWT will be carried out by using the relevant open code implemented on the samples domain (i.e. the support of the signal is the number of samples n; the scale in such circumstance is indicated by a). Due to the fast decay of the Gaussian wavelets in all calculations the infinite support of Gaussian wavelets (12) was assumed to be $[-5, 5]$.

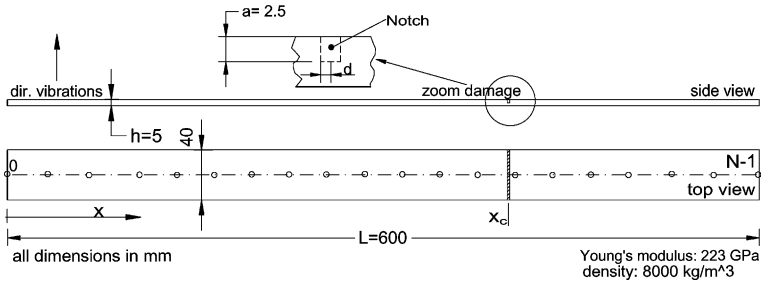

Fig. 4. Geometric, material characteristics and notations used for a beam model under investigation.

Table 1
First three natural frequencies [Hz] and percentage deviations for an undamaged and damaged beam (refer Fig. 4)

No.	Undamaged state (FF[a])	FF; $\xi_c = 0.5$	d (%)	FF; $\xi_c = 0.667$	d (%)	FF; $\xi_c = 0.85$	d (%)	CC; $\xi_c = 0.85$	d (%)
1	75.38	72.58	3.7	73.64	2.3	75.20	0.24	74.96	0.56
2	207.8	207.8	0.0	201.7	2.9	205.4	1.2	207.6	0.10
3	407.3	396.1	2.7	406.4	0.22	397.4	2.4	402.7	1.13

[a] Boundary conditions (F: free, C: clamped).

2.3. Crack and transversally vibrating beams modeling

In this section the signal that is going to be analyzed by CWT is elucidated. The signal is considered to be obtained by equally sampling the displacements at discrete points of a transversally vibrating beam (Fig. 4). Fig. 4 illustrates the cracked beam that here will be the main object of investigation. The damaged vibrating beam is modeled as a segmented beam whose analytical model was presented in Gentile and Messina (2002) and here it is referred to as a classical Eulero–Bernoulli beam model that neglects the rotatory inertia. The damage is simulated with an equivalent sub-beam having a different Young's module. In particular, Young's module is obtained through Eq. (13) that was obtained through a slightly modified model presented by Bovsunovsky and Matveev (2000), as reported in Gentile and Messina (2002).

$$\frac{E_{\mathrm{eq}}}{E} = \left[(1-\gamma)^3 + \frac{4.41}{12}\frac{(1-\gamma)}{d/h}\left[(1-\gamma)^6 - 3(1-\gamma)^2 + 2\right]\right]^{-1} \tag{13}$$

Based on Fig. 4, γ corresponds to the ratio $a/h = 0.5$ and d is representative of the half-width of the notch ($d = 1$ mm) which is located at the coordinate x_c.

As far as the simulated damaged scenario is concerned Table 1 has been taken into account. For the relevant mode shapes related to damaged conditions many authors have shown that visual inspections do not clearly show the damaged places and, therefore, an opportune digital signal processing of the discrete data (mode shape displacements whose maximum was scaled to 1) is clearly needed.

3. Detecting open cracks by using CWTs in uncontaminated data

In all the following simulations each single picture not only depicts the CWT $W(y(n), a)$ but also the analyzing wavelets. These are depicted in their supports through 2^8 grid points but scaled in the amplitude.

Such a representation clarifies the correlation evaluated by the wavelets when the damage is encountered during the convolution (i.e. Eqs. (3) and (4)). The finest scale in the samples domain was assumed to be $a = 1$ for all the Gaussian wavelets unless it is differently specified.

3.1. Equivalences among different families of wavelets

Fig. 5 first of all illustrates the capability of a Gaussian wavelet with *two* vanishing moments (Gaus 2) to correctly identify the damaged locations. As clarified in Section 2 the decay of $W(y(n), a)$ can be observed by reducing the scale a with the damage that is more accurately identified with an evident peak at the finest scale ($a = 2$).

Fig. 6 highlights how different families of wavelets such as Daubechies and Symlet (Daubechies, 1992) are also able to correctly identify the damaged locations. In particular, the wavelets represented in Fig. 6 have the same number of vanishing moments and different scales. The latter were chosen to get the same compact support for the analyzing wavelets. The coincidence of compact supports can be approximately verified by comparing the length of the wavelets depicted inside each single picture of Fig. 6. However, apart from the equivalence between the different wavelets depicted in Fig. 6, in this work only the Gaussian wavelets will be used for the theoretical advantages illustrated in Section 2.1.

Figs. 7–10 try to identify the damaged location by using the first 4 Gaussian wavelets. The scale was changed from $a = 3$ up to $a = 18{,}11$ through smaller steps than 15, 8. A smooth transition from sharp peaks ($a = 3$) to milder peaks ($a = 18{,}11$) was observed. Here, for brevity's sake, only extreme figures were reported. It is also interesting to verify how these four figures correspond just to the first four derivatives of the signal $y(x)$. However, it cannot be concluded that CWTs are equivalent to derivatives; at most the derivatives can be obtained as a particular case of the CWTs. The *equivalent derivatives* illustrated by Figs. 7–10 show how not only the second derivative deserves the attention (Pandey et al., 1991; Hoerst and Ratcliffe, 1997) of the analyst in order to locate a damaged zone. This was also pointed out from a numerical and an experimental point of view by the present investigators in a previous work (Gentile and Messina, 2002) who investigated higher order derivatives to locate damaged locations.

All the previous figures identify the location of damage with certain maxima that becomes thinner at the finest scale where, the identification seems to be the most accurate. These maxima propagate in the

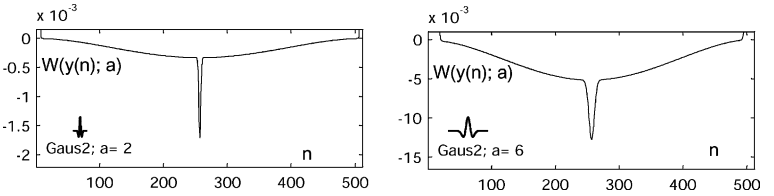

Fig. 5. CWTs for the first mode shape of a cracked FF-beam (refer Fig. 4). Crack at $n_c = 256$ or $\xi_c = x_c/L = 0.5$ (refer Table 1); $N = 512$.

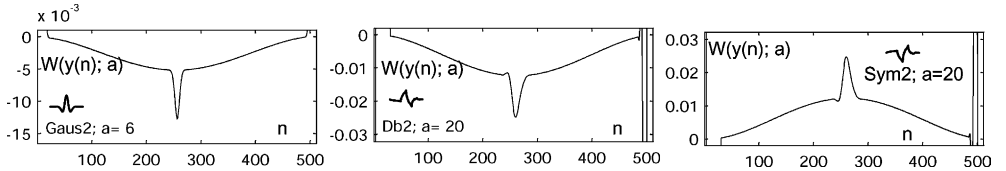

Fig. 6. CWTs for the first mode shape of a cracked FF-beam (refer Fig. 4) by using different wavelets mother. Crack at $n_c = 256$ or $\xi_c = x_c/L = 0.5$ (refer Table 1); $N = 512$.

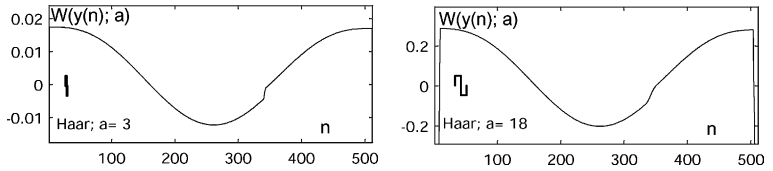

Fig. 7. CWTs for the second mode shape of a cracked FF-beam (refer Fig. 4) by using Haar wavelets mother. Crack at $n_c = 341$ or $\xi_c = x_c/L = 0.667$ (refer Table 1); $N = 512$.

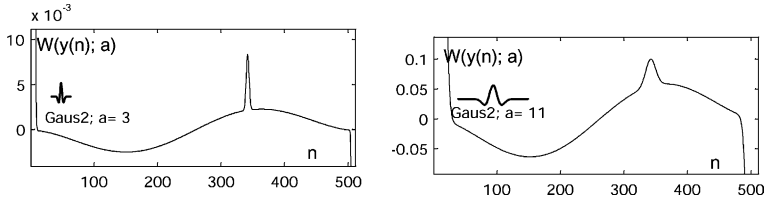

Fig. 8. CWTs for the second mode shape of a cracked FF-beam (refer Fig. 4) by using Gaus 2 wavelet mother. Crack at $n_c = 341$ or $\xi_c = x_c/L = 0.667$ (refer Table 1); $N = 512$.

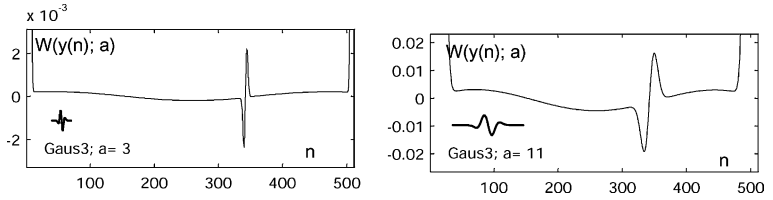

Fig. 9. CWTs for the second mode shape of a cracked FF-beam (refer Fig. 4) by using Gaus 3 wavelet mother. Crack at $n_c = 341$ or $\xi_c = x_c/L = 0.667$ (refer Table 1); $N = 512$.

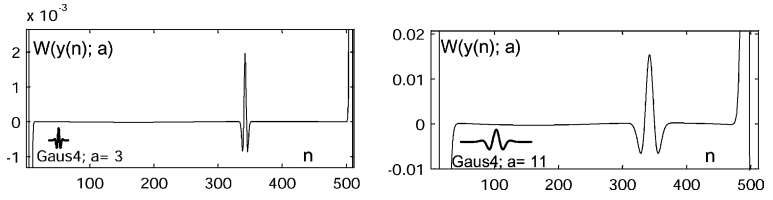

Fig. 10. CWTs for the second mode shape of a cracked FF-beam (refer Fig. 4) by using Gaus 4 wavelet mother. Crack at $n_c = 341$ or $\xi_c = x_c/L = 0.667$ (refer Table 1); $N = 512$.

damaged location with a typical cone as is shown in Fig. 11 where the absolute magnitude of different CWTs is mapped in a two-dimensional domain of samples and scales. This representation (Holschneider, 1995; Mallat, 2001), has been found to be less effective than Figs. 7–10. The effectiveness of Fig. 11 is strongly dependent on the colors used in the map besides being dependent on the boundary effects. Such boundary effect that was already mentioned in the introduction is mathematically elucidated in the following Section. Here, it is sufficient to state that certain boundary conditions of the beam can cause the CWT-values to be extremely high at the boundaries. Therefore, a color map scaled on the whole domain of the beam can make the *cone* correlating a true damaged location disappear. For this reason the boundaries in Fig. 11 were eliminated.

To conclude on the mentioned equivalencies between the CWT with derivative of a signal, it is natural to expect that the wavelets having only one vanishing moment cannot provide a peak in the damaged location.

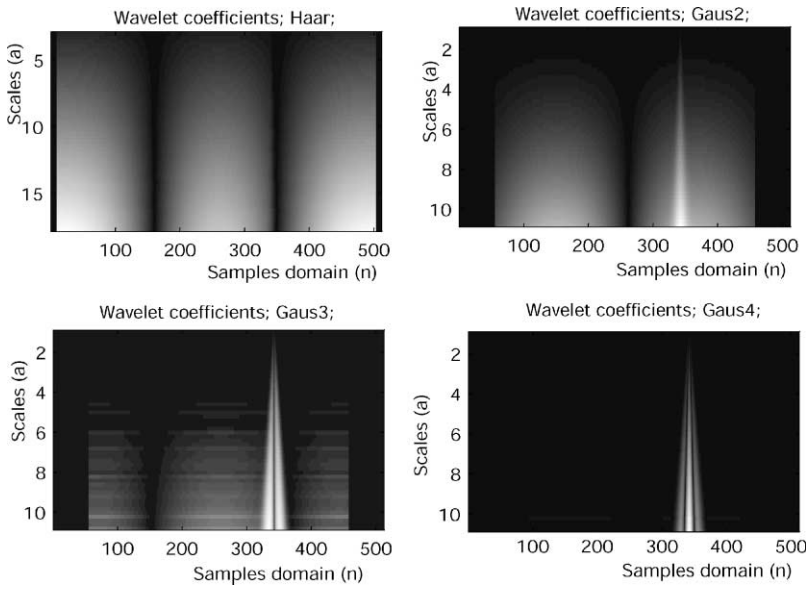

Fig. 11. Color maps of CWTs for the second mode shape of a cracked FF-beam (refer Fig. 4) by using different wavelets mother. Crack at $n_c = 341$ or $\xi_c = x_c/L = 0.667$ (refer Table 1); $N = 512$.

They indeed would provide, at a fixed scale, the first derivative, which, as is shown in Fig. 8, identify a damaged location with a *gap* rather than with a peak. A gap should be considered less effective than a peak (see also Fig. 11 concerned with Haar wavelets). Wang and Deng (1999) were able to find a crack through peaks by using a discrete Haar wavelet transform. Unfortunately, Wang and Deng (1999) did not detail the discrete numerical model they used and, therefore, a comparison of these two different perspectives was not attempted.

3.2. Boundary conditions: dependences and windowing as a possible remedy

This section is devoted to illustrate how, to a certain extent, the CWT is dependent on the boundary conditions. This dependence can be reduced by using concepts borrowed from digital signal processing techniques (e.g. Otnes and Enochson, 1978) in conjunction with the redundancy of the CWT (i.e. free choice of scales based on several wavelets).

In Fig. 12 the CWTs concerning the first three mode shapes of a damaged *clamped–clamped* beam have been depicted. The wavelet transforms of Fig. 12 were obtained by using the Gaus 2 wavelets. By comparing Fig. 12 with Figs. 5, 6 and 8 (FF-beam) it is evident that the localization follows similar performances. However, it is evident that Fig. 12 does not show an evident singularity at the boundaries. Conversely, at the boundaries of Figs. 5, 6 and 8 large values of CWTs occur. The larger the scale, the larger is the extension of such a boundary effect.

As previously stated, the large discrepancies occurring at the boundaries depend on the convolution operated by CWTs on $y(x)$ which is included into the infinite space. The large values at $x = 0, L$ are due to the presence of the discontinuity at those points. However, the discontinuities are of order 0 (discontinuous functions at $x = 0, L$) for a FF-beam whilst it is of order 2 (function and first derivative are continuous at $x = 0, L$) for a CC-beam. The milder discontinuity in CC-case evidently creates milder variations of the CWTs values at the boundaries.

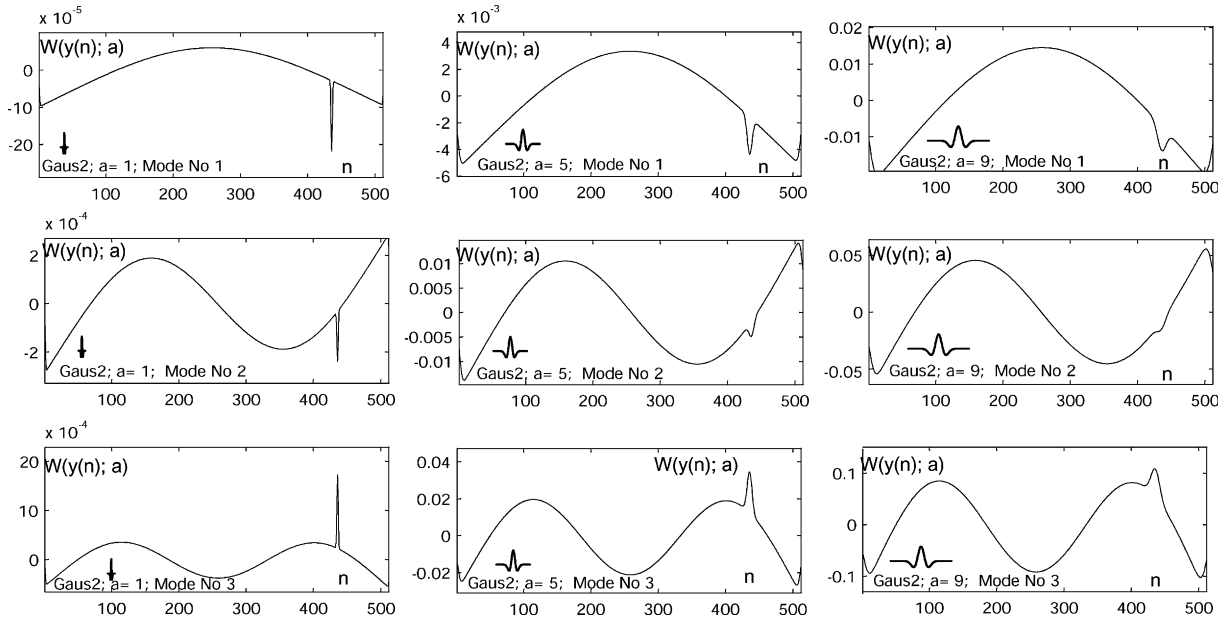

Fig. 12. CWTs for the first three mode shapes of a cracked CC-beam (refer Fig. 4) by using Gaus 2 wavelet mother. Crack at $n_c = 435$ or $\xi_c = x_c/L = 0.85$ (refer Table 1); $N = 512$.

This interpretation can be further justified by weighting the signal $y(x)$ through a window (e.g. Otnes and Enochson, 1978) that is able to smooth the discontinuity at the boundaries. Eq. (14) reports the Hanning window herein used to obtain the weighted signal $y(x)_w$.

$$w(x) = \frac{1 - \cos(2\pi x/L)}{2}; \qquad y(x)_w = w(x)y(x) \tag{14}$$

Such a window is able to enforce the continuity to an order 1 in the windowed signal $y(x)_w$. The enforcement to an order 2 can also be obtained by windowing the signal by using $w(x)^2$.

Fig. 13 illustrates how a CWT does not show large values at the boundaries of an FF beam when the signal $y(x)$ has previously been windowed through Hanning window. However, Fig. 13 also illustrates how the resolution for detecting damages through CWT undergoes the effect of the windows. With a Gaus 2 wavelet at its finest scale ($a = 1$) and by windowing the signal through $w(x)^2$ the localization near the boundaries is heavily deteriorated with respect to its relevant non-windowed case. In any case, the use of different wavelets also gives the possibility of extracting damage for heavily windowed signals ($w(x)^2$). Indeed, Fig. 14 illustrates how an analyzing wavelet characterized by a higher number of vanishing moments (Gaus 4) is able to extract a singularity by keeping the values low at the boundaries.

4. Detecting open cracks by using CWT with noisy data

This section illustrates the potentiality of the wavelets against data contaminated by noise.

In the following simulations the noise has been simulated by adding a Gaussian noise $n(x)$ to the true signal $y(x)_t$:

$$y(x) = y(x)_t + n(x)_{\mu,\sigma} \tag{15}$$

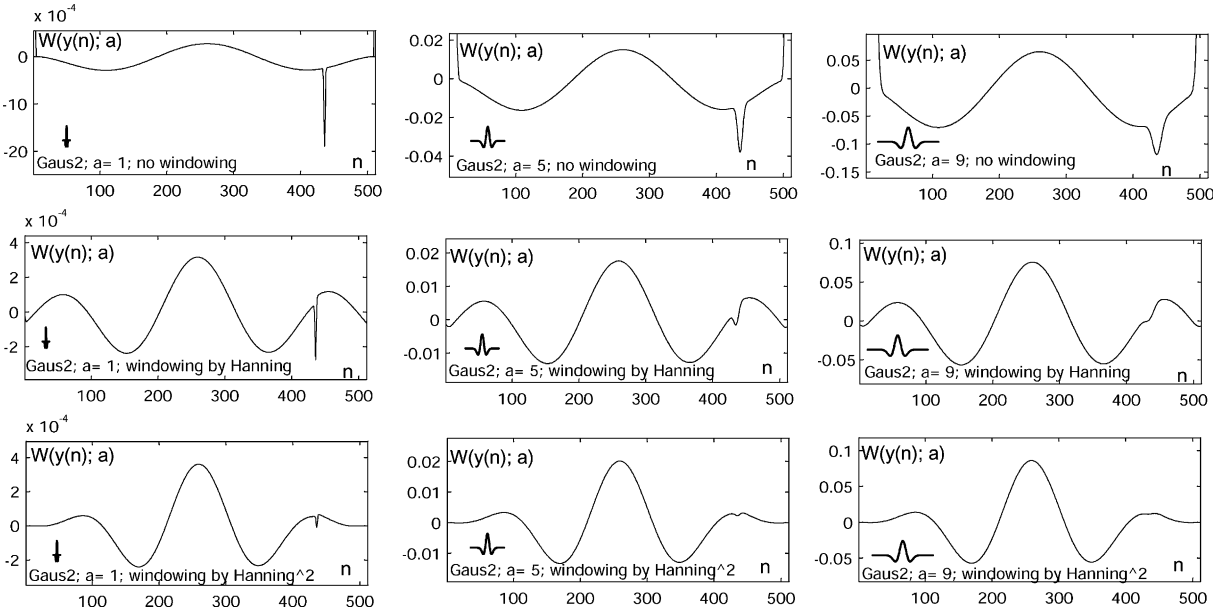

Fig. 13. CWTs for the third mode shape of a cracked FF-beam (refer Fig. 4) by using windowed mode shapes and Gaus 2 wavelet mother. Crack at $n_c = 435$ or $\xi_c = x_c/L = 0.85$ (refer Table 1); $N = 512$.

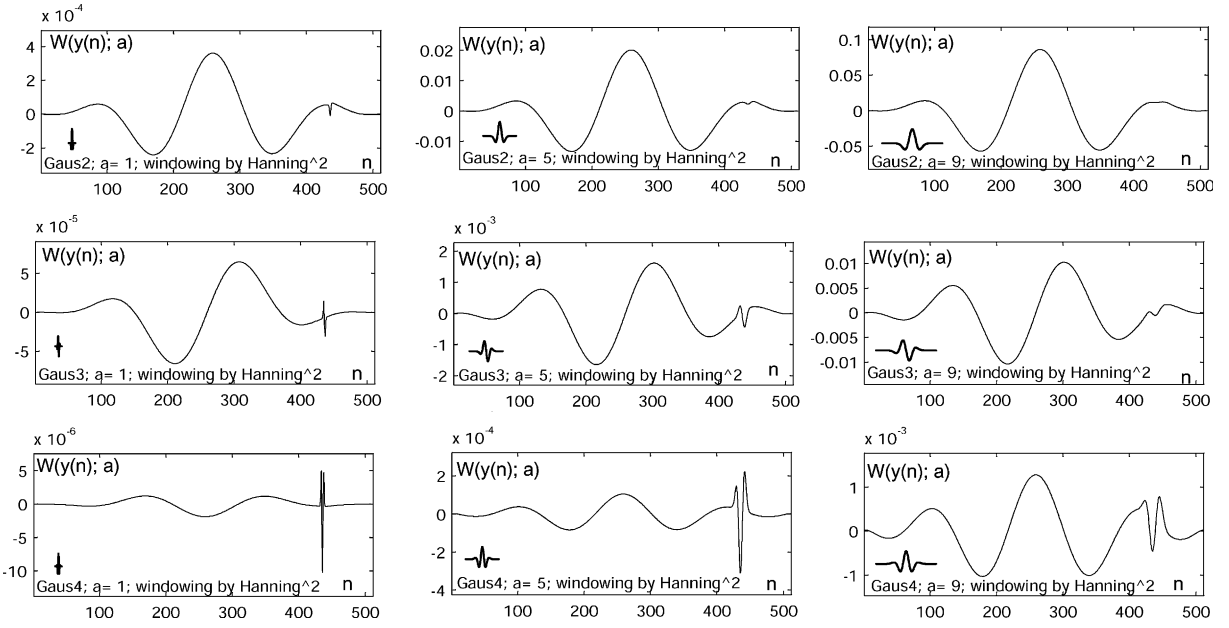

Fig. 14. CWTs for the third mode shape of a cracked FF-beam (refer Fig. 4) by using windowed mode shapes and different wavelets mother. Crack at $n_c = 435$ or $\xi_c = x_c/L = 0.85$ (refer Table 1); $N = 512$.

being μ and σ the mean and the standard deviation of the normal distribution respectively. The parameters (μ, σ) adopted in the simulations have been chosen by following Pai and Young (2001). As far as the *seed*

(Press et al., 1992) of the random distribution is concerned it was assumed to be constant for all the comparisons carried out. Additional tests based on different *seeds* values were also carried out; however, they were not reported for brevity's sake and they did not limit the relevant conclusions.

Based on the model established by Eq. (15), Fig. 15 illustrates the importance of taking into account the effect of noise. In particular, the top left of Fig. 15 depicts the second mode shape concerning a damaged condition. The mode shape has been illustrated as a signal free and contaminated by noise with a vertical shift by allowing a clearer comparison in both cases. From this graph it is clear that the noise does not seem to compromise the signal very much. However, the 3rd, and 4th derivatives of the signal $y(x)$ assessed by a finite difference scheme (Anderson et al., 1984, p. 45 by $O(h^2)$ with $h = 1$), highlights the importance to correctly processing the signal even when it contains a low level of noise. Indeed, those graphs illustrate how derivatives operations can enormously mask the damage in presence of contaminated data. On the other hand, the graph reported on the top right of Fig. 15 illustrates the capability of the third derivative to clearly locate the damage when applied on uncontaminated data.

Based on Section 2 it is interesting to raise the question whether the CWTs are submitted to the same disastrous effect to that of the derivatives (that is *mask effect*). In this respect Figs. 16 and 17 should be considered of main concern. These figures illustrate CWTs applied on two different mode shapes corresponding to two different damaged conditions (Table 1). Such figures illustrate that the CWT undergoes a mask effect at the finest scale ($a = 3$). This result does not come as a surprise for the reasons illustrated in Section 2. Indeed, when a scale value approaches to 0 the CWT theoretically approaches to a relevant derivative (Eq. (8)) that depends on the vanishing moments of the analyzing wavelet. In such a case it is reasonable to expect the presence of the mask effect obtained with the derivatives.

Therefore Figs. 16 and 17 suggest that the finest scale should not be generally considered as the best choice for accurately detecting damages when the signal is contaminated by noise. However, Figs. 16 and 17 also illustrate how a CWT is able to recover the part of interest from the signal (i.e. peaks corresponding to damaged locations) at higher scale values. Indeed, as the scale becomes higher, through finer steps of scales,

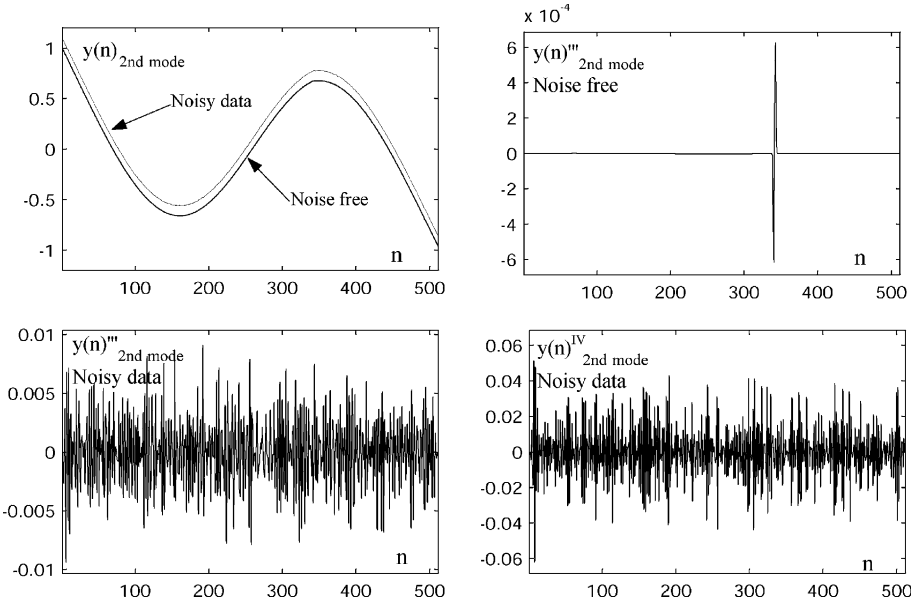

Fig. 15. Second mode shape of a cracked FF-beam (refer Fig. 4) with its 3rd and 4th derivative. Noise added to the mode shape: Gaussian, $\mu = 0$, $\sigma = 0.2\%$ of the maximum amplitude of the mode shape. Crack at $n_c = 341$ or $\xi_c = x_c/L = 0.667$ (refer Table 1); $N = 512$.

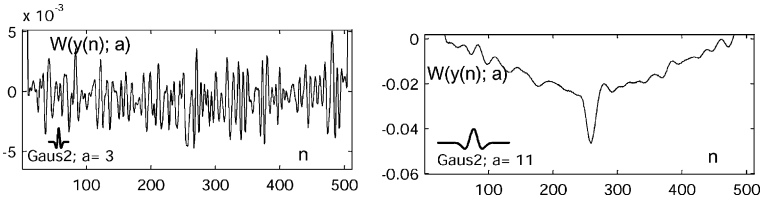

Fig. 16. CWTs for the first mode shape of a cracked FF-beam (refer Figs. 4 and 6) by using Gaus 2 wavelet mother. Noise added to the mode shape: Gaussian, $\mu = 0$, $\sigma = 0.2\%$ of the maximum amplitude of the mode shape.

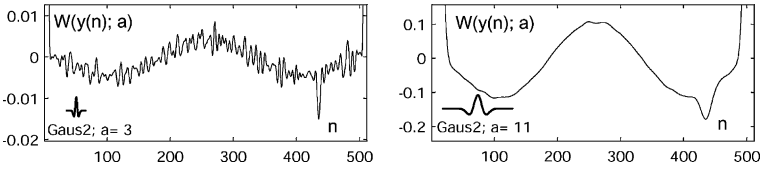

Fig. 17. CWTs for the third mode shape of a cracked FF-beam (refer Figs. 4 and 15) by using no windowing and Gaus 2 wavelet mother. Noise added to the mode shape: Gaussian, $\mu = 0$, $\sigma = 0.2\%$ of the maximum amplitude of the mode shape.

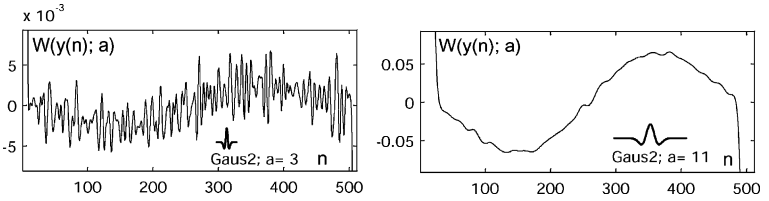

Fig. 18. CWTs for the second mode shape of a cracked FF-beam (refer Fig. 4) by using Gaus 2 wavelet mother. Crack at $n_c = 256$ or $\xi_c = x_c/L = 0.5$ (refer Table 1); $N = 512$. Noise added to the mode shape: Gaussian, $\mu = 0$, $\sigma = 0.2\%$ of the maximum amplitude of the mode shape.

the noise can be systematically seen as disappearing whilst the interesting part of the signal is preserved. Here only the first and last figures were retained for brevity's sake. This suggests that the wavelets not only include useful information related to the derivatives of a signal but they are also able to tackle signal contaminated by noise by adopting a tradeoff between finest scale and larger ones.

Fig. 18 illustrates the CWT obtained by convolving a mode shape whose relevant sensitivity (Table 1) is poor. In such a case the wavelets once again are able to clean the signal from the noise. However, a poor identification of the damaged location is shown. A similar result was also obtained with a damage occurring in a nodal point of the first mode shape. This suggests that the localization could be accomplished by using more than one single mode shape. In any case, whenever it is possible the natural frequency changes might be of support for the choice of the most sensitive mode shapes.

Figs. 19 and 20 analyze the same mode shapes of Figs. 16 and 17 in the same damaged conditions but by using Gaus 4 wavelets rather than Gaus 2. From Figs. 19 and 20 similar observations to these concerning Figs. 16 and 17 can be extracted. However, a request of higher scale values seems to be necessary with Gaus 4 to obtain the identification of damaged locations with the same accuracy as when using Gaus 2. This latter performance can be justified by using Property 1 by Eq. (4).

In this latter respect, the derivative operators in the transformed Fourier domain should first of all be taken into account. In particular, the derivative-operator into the Fourier domain can be seen as high-pass filters (e.g. Otnes and Enochson, 1978) with an amplification at higher frequencies. Therefore, the addition

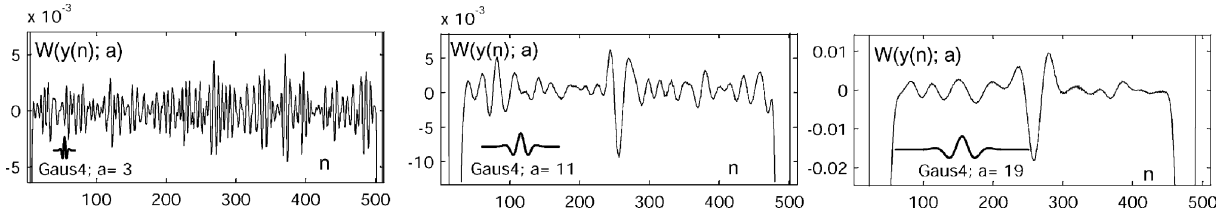

Fig. 19. CWTs for the first mode shape of a cracked FF-beam (refer Fig. 4) by using Gaus 4 wavelet mother. Crack at $n_c = 256$ or $\xi_c = x_c/L = 0.5$ (refer Table 1); $N = 512$. Noise added to the mode shape: Gaussian, $\mu = 0$, $\sigma = 0.2\%$ of the maximum amplitude of the mode shape.

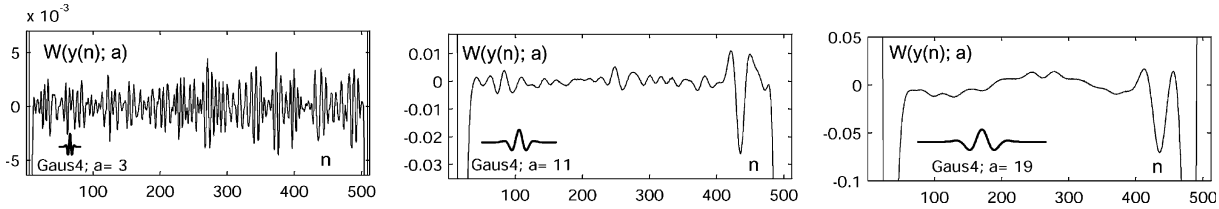

Fig. 20. CWTs for the third mode shape of a cracked FF-beam (refer Fig. 4) by using Gaus 4 wavelet mother. Crack at $n_c = 435$ or $\xi_c = x_c/L = 0.85$ (refer Table 1); $N = 512$. Noise added to the mode shape: Gaussian, $\mu = 0$, $\sigma = 0.2\%$ of the maximum amplitude of the mode shape.

of *high frequency* [2] noise on the low wavelength of the processed signal (i.e. mode shape or ODS) is naturally collected and amplified in the x-space by derivative-operators (Fig. 15). On the other hand, a wavelet, with an appropriate compact support in the Fourier domain (i.e. a band-pass filter), is able to reduce the noise thus preserving the interesting components of the signal. Indeed, from Eq. (4) it is clear that at high scales the Fourier transform of the wavelet is compressed in the frequency domain whilst the wavelet is dilated in the x-space. This explains how the noise is reduced at higher values of scales: the compression of wavelets in the Fourier domain transforms the wavelet into a narrow band-pass filter which selects from the signal components that are well localized in the Fourier domain. In such a case the broad band noise is reduced. This also supports the milder peaks obtained at higher scale values in all the damaged scenarios. In such a perspective, it is possible to explain the need for higher scale values when Gaus 4 (Figs. 19 and 20) is used in place of Gaus 2 (Figs. 17 and 18). In this respect Fig. 21 should be taken into account. Fig. 21(a) depicts the first four Gaussian wavelets and Fig. 21(b) illustrates the relevant Fourier transforms in an its classical form. Fig. 21(b) clearly shows that Gaus 4 is a band-pass filter differently located with respect to the band-pass filter related with Gaus 2. The former one clearly requires a higher compression (higher scale values) to let lower frequency noise pass.

A final test was retained worthy of attention to clarify the dependence of the performances of the CWTs on the number of points used to describe the discrete vibrational data (mode shapes or ODSs). In this respect Fig. 22 should be taken into account. Fig. 22 depicts the same mode shape (third one) related to a fixed damaged condition. A number of 64, 128, 256 and 512 points were used to describe the mode shape. Fig. 22 makes it clear that at a fixed length of the wavelet support the identification is not remarkably influenced. However, it should be considered that the present technique described in conjunction with Gaussian wavelets is mainly related with experimental techniques that are able to provide a reasonably high number of sampling points (e.g. Pai and Young (2001) illustrated how this is becoming a real technological

[2] In this work frequency (f) refers to the inverse of a wave length (length^{-1}).

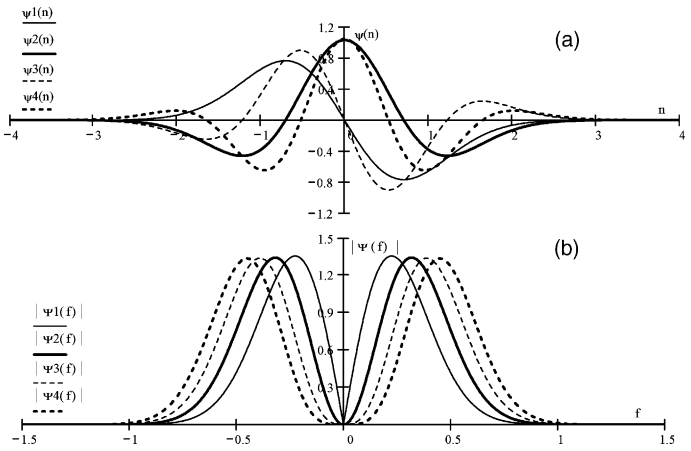

Fig. 21. First four Gaussian wavelets mother and related Fourier transforms.

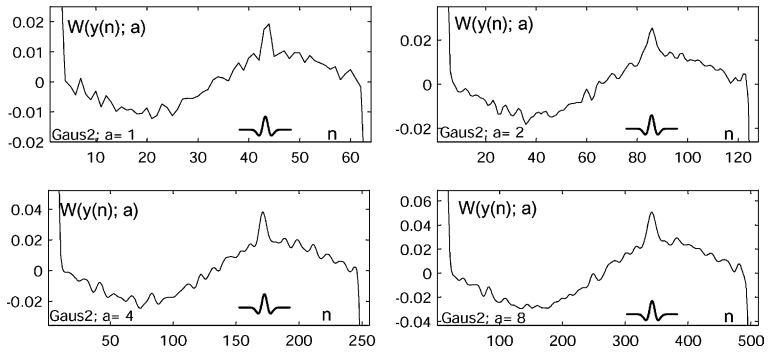

Fig. 22. CWTs for the third mode shape of a cracked FF-beam by using Gaus 2 wavelet mother with different number of sample points. Crack at $\xi_c = x_c/L = 0.667$ (refer Table 1). Noise added to the mode shape: Gaussian, $\mu = 0$, $\sigma = 0.2\%$ of the maximum amplitude of the mode shape.

possibility). In this respect, the shape of the wavelet mother needs a certain number of discrete points to be well described at its finest scale. This can become a difficult task for certain wavelets. For example, a wavelet Gaus 1 needs at least eleven points ($a = 1$) to be well described in the x-space. Similar observations apply to higher order Gaussian wavelets where higher scale values (higher sampling points per analyzing wavelet) are needed to represent the wavelets. When Gaus 2–4 are used, the eleven points related to the scale $a = 1$ already represent a minimum optimistic scale and higher values should be used. Therefore, because the end effect depends on the extension of the wavelets, there is a natural difficulty to process a low number of sampling points through classical Gaussian wavelets.

5. Closure and recommendations

In this work a thorough investigation on the applicability of certain recently proposed mathematical tools such as CWTs has been conducted for damage detection purposes of open cracks in transversally vibrating beams. The paper focused on the identification of damaged locations that could be considered of

primary importance in a diagnosing process. Its theoretical background has been extracted from the relevant literature for assisting the interpretation of each one of the presented results in both real (x-space) and transformed (Fourier-space) domain. The simulations carried out in conjunction with the theoretical background adopted have clarified that the CWTs are able to include in one only mathematical tool several mathematical features which are strictly related with the identification of damaged locations: derivatives, convolution and appropriate smoothing of noisy data. The simulations that have been conducted on free and noisy data have resulted in an excellent behavior of the CWTs in both cases. A list of the obtained results related to the Gaussian wavelets follows.

To a certain extent the CWTs are equivalent to the derivatives to which the merit to correctly identify the damaged locations intrinsically belongs. The analyst can approach a particular derivative by appropriately choosing the number of vanishing moments of a Gaussian wavelet.

In the presence of noise the finest scales cannot be generally considered the best choice. Indeed, in such a case the CWT includes all the disadvantages of the classical derivatives, which, behaving as high-pass filters in the Fourier-domain, mask the damage. On the other hand large scales lose the details. Therefore, to tackle noisy data through CWTs, a trade-off for the scale is needed.

Certain boundary conditions can reduce the effectiveness of the two-dimensional maps in order to detect the damaged locations. Windowing can reduce the boundary effect, but wavelets with a high number of vanishing moments should be preferred to insulate damaged locations close to the boundaries.

The redundancy (free choice of scales in conjunction with several wavelets) was observed to be an important factor in correctly detecting the damage. The CWTs should therefore be preferred with respect to the discrete wavelet transforms that cannot operate at every scale.

A fundamental mode shape cannot be considered more useful than higher modes when detecting the damage, nor can higher modes be considered more useful than a fundamental mode shape. The damage can be placed in locations having a poor sensitivity for certain mode shapes but higher for others. All the available mode shapes and/or ODSs should be analyzed when percentage natural frequency changes are not available.

Although the technique was based on a redundant number of discrete data points, which, are consistent with present vibration measurement systems, the simulations have shown a stable capability to detect the damage by also using a few discrete data.

It should be appreciated the effort of the present work that was conducted to collect under one unique perspective the several different attempts connected with the detection of cracks by using *spikes* in slopes through a characteristic shape of transversally vibrating beam.

The present investigation cannot be considered a conclusive work. Experimental tests are needed to demonstrate the real practicability of the method. In particular, experimental tests showing the sensitivity of the technique to detect damage at its early state are needed to illustrate how little the damage can be detected. The complexity of the matter alone deserves a dedicated investigation to consider damage minor than the 50% thickness reduction as well as considering different typology of damage on real systems. These experimental tests would also provide a useful correlation with the study carried out in this work. Finally, additional work in the transformed Fourier domain is expected to further elucidate the results obtained in the present investigation.

Acknowledgements

The ContentsDirect from Elsevier Science service is acknowledged for bringing to the attention of the authors the work by Hong et al. (2002), which electronically appeared just two days before submitting the present manuscript (issue of April 2002). The authors are also grateful to Dr. Manlio Tesauro of the University of Lecce, for the interesting discussions on the wavelets.

References

Anderson, D.A., Tannehill, J.C., Pletcher, R.H., 1984. Computational Fluid Mechanics and Heat Transfer. Hemisphere Publishing Corporation, New York.

Bovsunovsky, A.P., Matveev, V.V., 2000. Analytical approach to the determination of dynamic characteristics of a beam with a closing crack. Journal of Sound and Vibration 235 (3), 415–434.

Chance, J., Thomlinson, G.R., Worden, K., 1994. A simplified approach to the numerical and experimental modelling of the dynamics of a cracked beam. In: 12th International Modal Analysis Conference, Honolulu, USA, pp. 778–785.

Daubechies, I., 1992. Ten Lectures on Wavelets. SIAM, Philadelphia, PA.

Doebling, S.W., Farrar, C.R., Prime, M.B., 1998. A summary review of vibration-based damage identification methods. The Shock and Vibration Digest 30 (2), 91–105.

Døssing, O., Staker, C.H., 1987. Operational deflection shapes: background, measurement and applications. In: 5th International Modal Analysis Conference, London, UK, pp. 1372–1378.

Ewins, D.J., 1992. Modal Testing: Theory and Practice. John Wiley, New York.

Gentile, A., Messina, A., 2002. Detection of cracks by only measured mode shapes in damaged conditions. In: 3rd International Conference on Identification in Engineering Systems, Swansea, Wales.

Haar, A., 1910. Zur theorie der orthogonalen funktionensysteme. Mathematische Annalen 69, 331–371.

Hoerst, B.C., Ratcliffe, C.P., 1997. Damage detection in beams using laplacian operators on experimental modal data. In: 15th International Modal Analysis Conference, Orlando, USA, pp. 1305–1311.

Holschneider, M., 1995. Wavelets an Analysis Tool. Clarendon Press, Oxford.

Hong, J.C., Kim, Y.Y., Lee, H.C., Lee, Y.W., 2002. Damage detection using the Lipschitz exponent estimated by the wavelet transform: applications to vibration modes of a beam. International Journal of Solids and Structures 39, 1803–1816.

Jauregui, D.V., Farrar, C.R., 1996. Comparison of damage identification algorithms on experimental modal data from a bridge. In: 14th International Modal Analysis Conference, pp. 1423–1429.

Lu, C.J., Hsu, Y.T., 1999. Application of wavelet transform to structural damage detection. In: 17th International Modal Analysis Conference, Kissimee, USA, pp. 908–914.

Mallat, S., Hwang, W.L., 1992. Singularity detection and processing with wavelets. IEEE Transactions on Information Theory 38 (2), 617–643.

Mallat, S., 2001. A Wavelet Tour of Signal Processing. Academic Press, New York.

McHargue, P.L., Richardson, M.H., 1993. Operating deflection shapes from time versus frequency domain measurements. In: 11th International Modal Analysis Conference, Kissimmee, USA, pp. 581–587.

Messina, A., Williams, E.J., Contursi, T., 1998. Structural damage detection by a sensitivity and statistical-based method. Journal of Sound and Vibration 216 (5), 791–808.

Misiti, M., Misiti, Y., Oppenheim, G., Poggi, J.M., 1996. Wavelet Toolbox for use with MATLAB®. The MathWorks Inc., Natick.

Naldi, G., Venini, P., 1997. Wavelet analysis of structures: statics, dynamics and damage identification. Meccanica 32, 223–230.

Otnes, K.R., Enochson, L., 1978. In: Applied Time Series Analysis, vol. 1. John Wiley and Sons, New York.

Pai, P.F., Young, L.G., 2001. Damage detection of beams using operational deflection shapes. International Journal of Solids and Structures 38, 3161–3192.

Pandey, A.K., Biswas, M., Samman, M.M., 1991. Damage detection from changes in curvature mode shapes. Journal of Sound and Vibration 145 (2), 321–332.

Press, W.H., Teukolsky, S.A., Vetterling, W.T., Flannery, B.P., 1992. Numerical Recipes in C. Cambridge University Press, Cambridge.

Quek, S.T., Wang, Q., Zhang, L., Ang, K.K., 2001. Sensitivity analysis of crack detection in beams by wavelet technique. International Journal of Mechanical Sciences 43, 2899–2910.

Ratcliffe, C.P., Bagaria, W.J., 1998. Vibration technique for locating delamination in a composite beam. American Institute of Aeronautics and Astronautics Journal 36 (6), 1074–1077.

Stubbs, N., Osegueda, R., 1990. Global non destructive damage evaluation in solids. International Journal of Analytical and Experimental Modal Analysis 5 (2), 67–79.

Surace, C., Ruotolo, R., 1994. Crack detection of a beam using the wavelet transform. In: 12th International Modal Analysis Conference, Honolulu, USA, pp. 1141–1147.

Wang, Q., Deng, X., 1999. Damage detection with spatial wavelets. International Journal of Solids and Structures 36, 3443–3468.

Yuen, M.M.F., 1985. A numerical study of the eigenparameters of a damaged cantilever. Journal of Sound and Vibration 103 (3), 301–310.